Crystal and electronic structures of Tris[4,4,4-Trifluoro-1-(2-X)-1,3-butanedionato]iron(III) isomers (X = thienyl or furyl): an X-ray and computational study

Marrigje M. Conradie,[a] Petrus.H.van Rooyen,[b] Jeanet Conradie[a,*]

[a] Department of Chemistry, PO Box 339, University of the Free State, 9300 Bloemfontein, Republic of South Africa.

[b] Department of Chemistry, University of Pretoria, Private Bag X20, Hatfield, 0028, South Africa.

*Contact author details:

Jeanet Conradie

Tel: +27-51-4012194

Fax: +27-51-4446384

e-mail: conradj@ufs.ac.za

Keywords

iron(III), β-diketone, structure

Graphical abstract

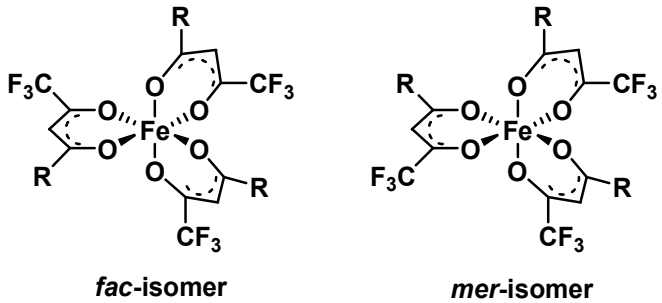

Synopsis

Electronic and crystal structures of selected *fac* and *mer* isomers of tris(beta-diketonato)$_3$ complexes.

Highlights

Crystal structures of *fac* and *mer* isomers of tris(beta-diketonato)$_3$ complexes.

DFT calculations showed that the *mer* isomers are energetically favoured for both complexes.

Molecular energy levels and orbitals of [Fe(acac)$_3$].

DFT calculations showed that complex [Fe(acac)$_3$] is high-spin and exhibits a negative D_3 distortion from the octahedral ligand field.

Abstract

DFT calculations showed that [Fe(acac)$_3$] (where acac = acetylacetonato) is high-spin, with a negative D_3 distortion from the octahedral ligand field. Calculations further showed that, although both the *fac* and *mer* isomers of complexes [Fe($CF_3COCHCOR$)$_3$], where R = C_4H_3S or C_4H_3O, can exist, the *mer* isomers are energetically favoured in both complexes. The structure of the major *mer* isomer of [Fe($CF_3COCHCOC_4H_3S$)$_3$] has been published previously, while the crystal structure of the minor *fac* isomer of [Fe($CF_3COCHCOC_4H_3S$)$_3$] is presented in this study. The structure of the *mer* isomer of [Fe($CF_3COCHCOC_4H_3O$)$_3$], in agreement with DFT calculations, showed that the furyl substituent pointed towards the CF_3 group in a *syn* orientation.

1 Introduction

In organic chemistry, complex tris(acetylacetonato)iron(III) or [Fe(acac)$_3$], has been explored as a catalyst and reagent in many reactions. For example, [Fe(β-diketonato)$_3$] has been found to catalyze the reaction of N-sulfonyl oxaziridines with olefins to form 1,3-oxazolidine products [1]; to catalyze the dimerization of isoprene to a mixture of 1,5-dimethyl-1,5-cyclooctadiene and 2,5-dimethyl-1,5-cyclooctadiene [2]; to catalyze the cross-coupling reaction of Grignard reagents with alkyl halides [3]; to catalyze the acylation of Grignard reagents [4]; and to catalyze the ring-opening polymerization of 1,3-benzoxazine [5]. In the latter case, it has been found that by replacing the acetylacetonato ligand by hexafluoroacetylacetonato, the activity of the iron complex was remarkably enhanced [5]. From the various iron(III) complexes examined in the cross-coupling reaction of Grignard reagents with alkyl halides, [Fe(dibenzoylmethanato)$_3$] was found to be the

most effective, as far as rates and deactivation [6] are concerned. Effective catalyst design should focus on factors such as catalyst efficiency, costs, toxicological benignity, environmental friendliness and long-term stability. It therefore is necessary to continuously study the basic structure and properties of complexes related to known catalysts.

In this contribution we present the synthesis, structure and properties of two [Fe(β-diketonato)$_3$] complexes: where β-diketonato = 4,4,4-Trifluoro-1-(2-thienyl)-1,3-butanedione, abbreviated as tta (**1**); and 4,4,4-Trifluoro-1-(2-furyl)-1,3-butanedione, abbreviated as tffu (**2**). For these β-diketonato-iron(III) complexes, with a unsymmetrical β-diketone ligand, two stereo isomers are possible: a facial isomer (*fac*) and a meridional isomer (*mer*); see Scheme 1. The ligands in the facial isomer are arranged symmetrically around the metal, while the ligands in the meridional isomer are arranged in such a way that one ligand is unsymmetrical.

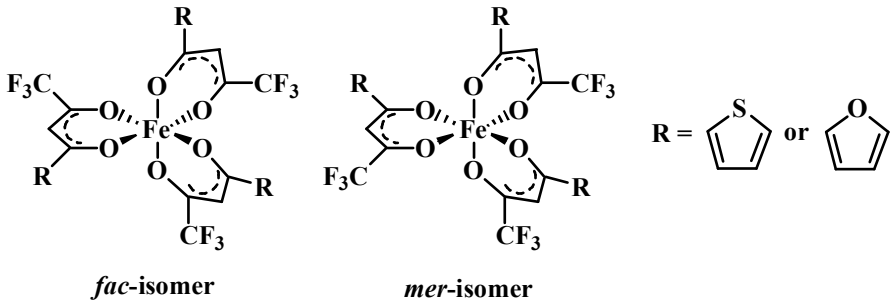

Scheme 1: The facial (*fac*) and meridional (*mer*) isomers of [Fe(β-diketonato)$_3$] complexes, with unsymmetrical β-diketonato ligands, where R = C_4H_3S (**1**) or C_4H_3O (**2**).

2 Experimental

2.1 Material and methods

Reagents were obtained from Merck and Sigma-Aldrich. Solid reagents employed in preparations were used directly, without further purification. Liquid reactants and solvents were distilled prior to use. Doubly distilled H_2O was used. Organic solvents were dried and distilled before use. Melting points (m.p.) were determined by an Olympus BX51 system microscope, assembled on top of a Linkam THMS600 stage, and connected to a Linkam TMS94 temperature programmer. Elemental analysis was performed by Canadian Microanalytical Service Ltd, Canada. MALDI-TOF-MS (matrix assisted laser desorption/ionization time-of-flight mass spectrometry) spectra were collected by a Bruker Microflex LRF20, in the negative and positive reflection mode (independently), using the minimum laser power required to observe signals.

The β-diketones used in this study were obtained from Merck and Sigma-Aldrich. Both [Fe(β-diketonato)$_3$] complexes were prepared by an adapted procedure [7,8].

[Fe(tta)$_3$] (**1**): A metal solution of 0.15 mmol $Fe(NO_3)_3.9H_2O$ (dissolved in 10 ml H_2O) was buffered with 0.45 mmol $CH_3COONa.3H_2O$ (dissolved in 10 ml H_2O). To this buffered metal solution, a 0.53 mmol β-diketone (Htta) solution was added (solid Htta dissolved in 10 ml EtOH). The resulting solution was stirred well for 30 minutes and left overnight in a fume hood. The precipitate was collected by filtration and washed with H_2O. Yield 78%. Colour: dark red. M.p. 158.0–161.0 °C (reported: 159–160 °C [7], 162.5 °C [9]). UV: λ_{max} 333 nm, ε_{max} 48461 $mol^{-1}.dm^3.cm^{-1}$ (CH_3CN). MS Calcd. ([M], negative mode): *m*/*z* 719.4. Found: *m*/*z* 718.9. Anal. Calcd. for $FeC_{24}H_{12}S_3O_6F_9$: C, 40.07; H, 1.68. Found: C, 39.51; H, 1.70.

[Fe(tffu)$_3$] (**2**): A metal solution of 0.15 mmol $Fe(NO_3)_3.9H_2O$ was buffered with 0.45 mmol $CH_3COONa.3H_2O$ (dissolved in minimal H_2O). To this, EtOH was added to produce a 1 : 1 H_2O : EtOH solution. With the aid of a syringe, liquid 0.53 mmol β-diketone (Htffu) was added. The resulting solution was stirred well (with a lid on) for 30 minutes and left overnight in a fume hood (without lid). The precipitate was collected by filtration and washed with H_2O. Yield 92%. Colour: dark red. M.p. 205.0–208.0 °C (reported: 201–208 °C [7]). UV: λ_{max} 333 nm, ε_{max} 53476 $mol^{-1}.dm^3.cm^{-1}$ (CH_3CN). MS Calcd. ([M], positive mode): *m*/*z* 671.2. Found: *m*/*z* 671.1. Anal. Calcd. for $FeC_{24}H_{12}O_9F_9$: C, 42.95; H, 1.80. Found: C, 42.91; H, 1.83.

Density functional theory (DFT) calculations were carried out, using the ADF (Amsterdam Density Functional) 2012 programme [10], with a selection of GGA (Generalized Gradient Approximation) functionals, namely PW91 (Perdew-Wang 1991) [11], BP86 (Becke-Perdew) [12,13], and OLYP (Handy-Cohen and Lee-Yang-Parr) [14,15], as well as the hybrid functional B3LYP (Becke 1993 and Lee-Yang-Parr) [16,17]. The TZP (Triple ζ polarized) basis set, with a fine mesh for numerical integration, a spin-unrestricted formalism and full geometry optimization, applying tight convergence criteria, was used for minimum energy searches. Scalar relativistic effects, with the ZORA (Zero Order Regular Approximation) formalism [18,19,20,21,22], were included for all optimizations.

2.2 Crystal structure analysis

Data for red crystals of [Fe(tta)$_3$] (**1**, isomer *fac*) and [Fe(tffu)$_3$] (**2**, isomer *mer*), obtained from solutions in diethyl ether, were collected on a Bruker D8 Venture kappa geometry diffractometer, with duo Iμs sources, a Photon 100 CMOS detector and APEX II [23] control software using Quazar multi-layer optics monochromated, Mo-*K*α radiation by means of a combination of ϕ and ω scans. Data reduction was performed using SAINT+ [23] and the intensities were corrected for absorption using SADABS [23]. The structure was solved by intrinsic phasing using SHELXTS and refined by full-matrix least squares, using SHELXTL + [24] and SHELXL-2013+ [24]. In the

Table 1: Selected crystal data, data collection and structure refinement details of [Fe(tta)$_3$] (**1**, isomer *fac*) and [Fe(tffu)$_3$] (**2**, isomer *mer*).

Complex	[Fe(tta)$_3$] (**1**, isomer *fac*)	[Fe(tffu)$_3$] (**2**, isomer *mer*)
Empirical formula	$C_{24}H_{12}F_9FeO_6S_3$	$C_{24}H_{12}F_9FeO_9$
Formula weight	719.37	671.19
Temperature (K)	150(2)	150(2)
Crystal system	Trigonal	Monoclinic
Space group	R -3 :H	P 2_1/c
Unit cell dimensions (Å, °)	a = 18.2545(10)	a = 10.2891(5)
	b = 18.2545(10)	b = 17.9825(8)
	c = 14.2292(7)	c = 13.7620(7)
	α = 90	α = 90
	β = 90	β = 98.054(2)
	γ = 120	γ = 90
Volume (Å^3)	4106.3(5)	2521.2(2)
Z	6	4
Density (calc) (Mg/m^3)	1.745	1.768
Absorption coeff (mm^{-1})	0.881	0.719
F(000)	2154	1340
Crystal size (mm^3)	0.255 x 0.030 x 0.028	0.420 x 0.368 x 0.230
Theta range, data collection (°)	2.948 to 26.367	2.265 to 26.371
Reflections collected	57672	92527
Independent reflections	1863 [R(int) = 0.0597]	5144 [R(int) = 0.0505]
Absorption correction	Semi-empirical from equivalents	
Refinement method	Full-matrix least-squares on F^2	
Data / restraints / parameters	1863 / 0 / 126	5144 / 0 / 388
Goodness-of-fit on F^2	1.127	1.206
Final R indices [I>2σ(I)]	R1 = 0.778, wR2 = 0.2176	R1 = 0.0762, wR2 = 0.1826
R indices (all data)	R1 = 0.0836, wR2 = 0.2227	R1 = 0.0839, wR2 = 0.1866
Largest diff. peak, hole (e.Å^{-3})	1.994 and -0.852	0.192 and -0.469

structure refinement, all hydrogen atoms were added in calculated positions and treated as riding on the atom to which they are attached. All non-hydrogen atoms were refined with anisotropic displacement parameters, except C5 in [Fe(tta)$_3$] (**1**), all isotropic displacement parameters for hydrogen atoms were calculated as X × Ueq of the atom to which they are attached, where X = 1.5 for the methyl hydrogens and 1.2 for all other hydrogens. Crystal data and structural refinement parameters are summarized in Table 1.

3 Results and Discussion

3.1 Molecular structures of [Fe(tta)$_3$] (1, isomer fac*) and [Fe(tffu)$_3$] (2, isomer* mer*)*

Perspective drawings [25] of the molecular structures of [Fe(tta)$_3$] (**1**, isomer *fac*) and [Fe(tffu)$_3$] (**2**, isomer *mer*), showing the crystallographic numbering scheme used, are presented in Figure 1 and Figure 2. Diffraction quality crystals of [Fe(tta)$_3$] and [Fe(tffu)$_3$] were obtained, with some difficulty, from saturated solutions in diethyl ether at < 273 K. [Fe(tta)$_3$] (**1**) crystallized in a trigonal space group, with the site occupancy of the octahedral Fe-atom in the asymmetric unit being 1/3. The cyclic Fe–O–C–C–C–O fragment is planar, with the S-atom of the thienyl ring pointing in the opposite direction as the CF_3 group, thus being in an *anti*-orientation. This orientation also has been observed previously in the *mer* geometry of [Fe(tta)$_3$] [9]. There is some indication of site disorder, due to the possibility of the thienyl ring being present in two different orientations. Due to the quality of the crystal data, it has not been possible to determine a realistic model, incorporating both possible *anti* and *syn* orientations in the refinement, even though the difference electron density map did reveal a suitable peak at a distance of 0.45 Å from C5. Models that were investigated in refining the S1 : C5 ratio, suggested that the ratio of the two orientations of the structure, as presented in Figure 1, was more than 80 : 20. The solution with the best refined structure resulted from refining the C5 atom isotropically, which is the orientation presented in Figure 1. The structure of [Fe(tffu)$_3$] (**2**) revealed that the orientation of the oxygen atom in the furyl substituent pointed towards the CF_3 group in a *syn* orientation, with no indication of any site disorder, similar to what has been observed for [Fe(tta)$_3$]. Structural parameters of importance are summarized in

Table 2. The cyclic Fe–O–C–C–C–O fragment in [Fe(tta)$_3$] is close to planarity, with the RMS for the mean plane through this fragment being 0.0290 and the largest deviation from planarity being 0.047(2) Å for O1. In [Fe(tffu)$_3$], the three independent cyclic fragments have RMS values of 0.0787 for ring1 (Fe1–O1–C1–C2–C3–O2), 0.0782 for ring2 (Fe1–O3–C4–C5–C6–O4) and 0.0392

for ring3 (Fe1–O5–C7–C8–C9–O6). The largest deviation from planarity is 0.110(2) Å for Fe1 in ring1, 0.111(3) Å for O4 in ring2 and 0.064(3) Å for O6 in ring3. The angles between t

Table 2: Selected geometric parameters for **1** (isomer *fac*) and **2** (isomer *mer*).

Bond length (Å)	**1** (isomer *fac*) [a]	**2** (isomer *mer*)
Fe1–O1	1.975(3)	2.011(4)
Fe1–O2	1.996(3)	1.985(4)
Fe1–O3		2.004(3)
Fe1–O4		1.993(4)
Fe1–O5		2.009(4)
Fe1–O6		1.980(4)
Bond angle (°)		
O1–Fe1–O2	87.44(12)	87.28(14)
O1–Fe1–O3		93.01(14)
O1–Fe1–O4		85.38(15)
O1–Fe1–O5		89.09(15)
O1–Fe1–O6		176.49(15)
O1–Fe1–O1#1	91.23(13)	
O1#2–Fe1–O2#2	88.48(12)	
O1#2–Fe1–O2#1	92.95(13)	
O1–Fe1–O2#1	175.63(12)	
Torsion angle (°)		
Fe1–O1–C1–C2	7.6(7)	-11.6(7)
Fe1–O2–C3–C2	0.6(6)	10.4(7)
O1–C1–C2–C3	-1.6(7)	-1.5(8)
C1–C2–C3–C4	177.0(4)	
C8–C1–C2–C3	-178.6(4)	
C14–C3–C2–C1		-178.8(5)
C3–C2–C1–C10		178.8(4)

a Symmetry transformations used to generate equivalent atoms: **#1:** -y+1,x-y,z **#2:** -x+y+1,-x+1,z

hese rings vary between 80.1(1)–82.8(1)°. It also is of interest, that the O–Fe–O(*cis*) bond angles

vary between 87.44–92.95° in [Fe(tta)$_3$] and between 85.38–94.08° in [Fe(tffu)$_3$]. The O–Fe–O(*trans*) bond angle is 175.63° in [Fe(tta)$_3$] and varies between 171.20–177.71° in [Fe(tffu)$_3$]. The crystal packing of [Fe(tta)$_3$] (**1**, isomer *fac*) and [Fe(tffu)$_3$] (**2**, isomer *mer*) is displayed respectively in Figure 3 and Figure 4. There are some moderate π-stacking effects present in [Fe(tta)$_3$], with the distance between the parallel thienyl rings at 3.560 Å. The packing of [Fe(tffu)$_3$] does not display

similar π-stacking effects, but shows that the octahedral Fe–O core, together with the CF_3 groups, forms approximate channels during packing.

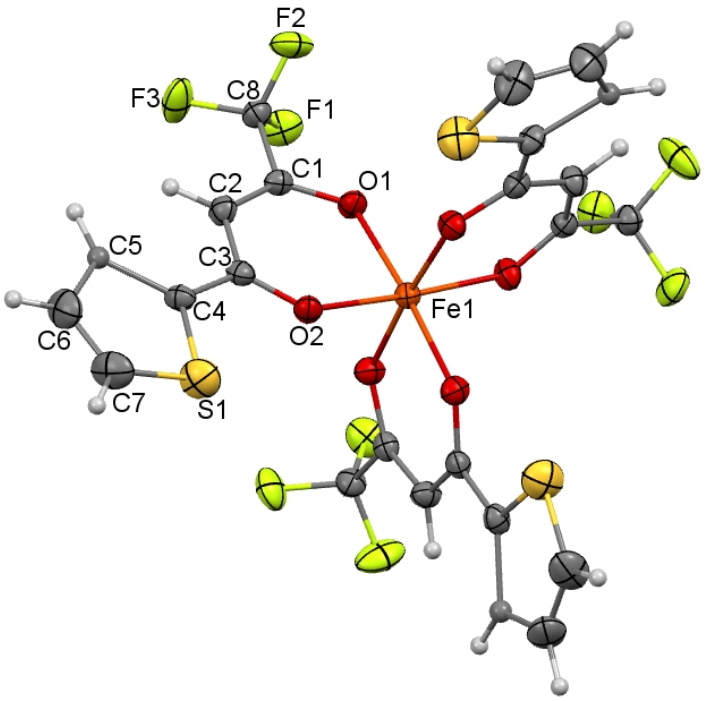

Figure 1: A perspective drawing of the molecular structure of [Fe(tta)$_3$] (**1**, isomer *fac*), showing the atom numbering scheme. ADPs are shown at the 50 % probability level.

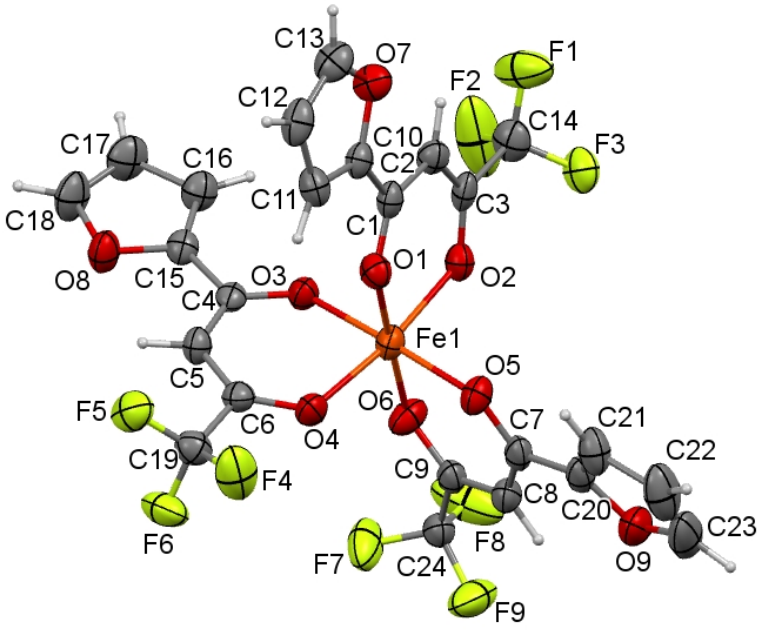

Figure 2: A perspective drawing of the molecular structure of [Fe(tffu)$_3$] (**2**, isomer *mer*), showing the atom numbering scheme. ADPs are shown at the 50 % probability level.

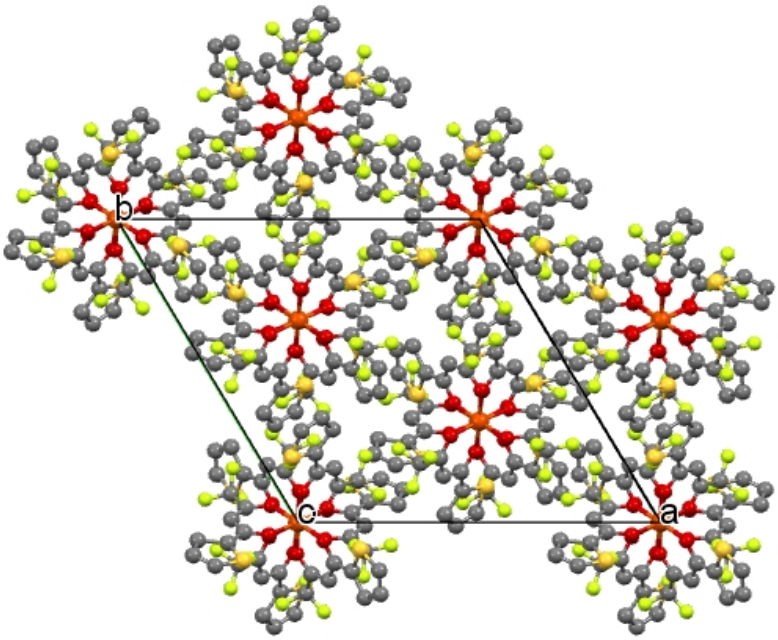

Figure 3: The molecular packing of $[Fe(tta)_3]$ (**1**, isomer *fac*), viewed along the c-axis.

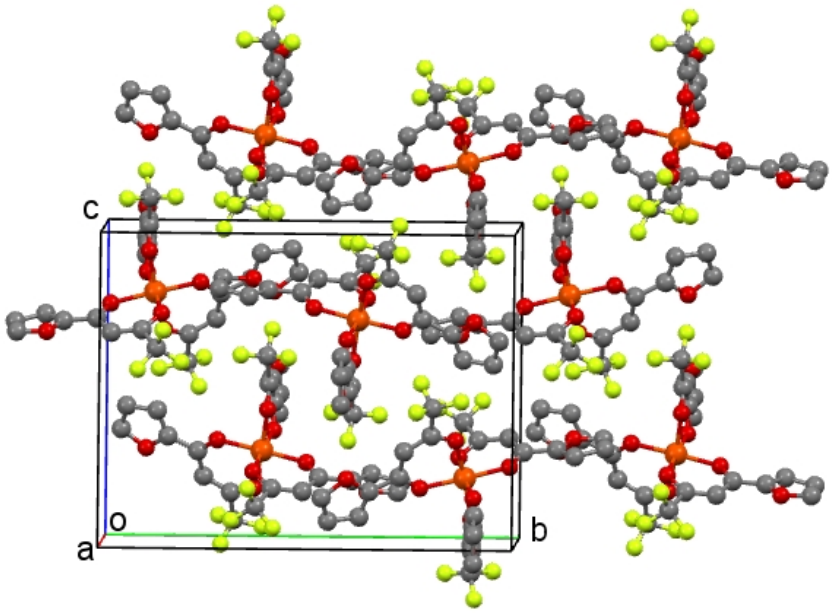

Figure 4: The molecular packing of $[Fe(tffu)_3]$ (**2**, isomer *mer*), viewed along the a-axis.

3.2 Computational chemistry study

Tris(β-diketonato) iron(III) complexes are stable molecules, with the metal in a high-spin state (S = 5/2) [26,27,28]. These complexes can either have a D_3, C_3 or C_1 symmetry: D_3 symmetry for complexes with symmetrical β-diketone ligands, *e.g.* $[Fe(acac)_3]$; C_3 symmetry for complexes with unsymmetrical β-diketone ligands, arranged in such a way that they have a 3-fold rotational axis, *e.g.* the *fac* isomers of (**1**) and (**2**); or C_1 symmetry for complexes with unsymmetrical β-diketone ligands, arranged in such a way that they have no symmetry operation, *e.g.* the *mer* isomers of (**1**)

and (**2**). In this section, the computational chemistry results of complex [Fe(acac)$_3$] and both the *fac* and *mer* isomers of [Fe(tta)$_3$] (**1**) and [Fe(tffu)$_3$] (**2**) will be presented and compared to experimental data. Since C_3 symmetry has complex irreducible representations which have not been implemented in ADF 2012 [10], C_1 symmetry was used in the calculations for both the *fac* and *mer* isomers of (**1**) and (**2**).

The reliable prediction of the spin ground-state of iron complexes is notoriously difficult and the applicability of various functionals and basis sets has been studied by various authors [29**].** It is thus of importance to choose a functional-basis set combination that give a reliable spin state and geometry description of tris(β-diketonato) iron(III) complexes. To validate the accuracy of the DFT calculated energies, all the states S = 1/2, 3/2 and 5/2, of [Fe(acac)$_3$], and the *fac* and *mer* isomers of [Fe(tta)$_3$] (**1**) and [Fe(tffu)$_3$] (**2**), were optimized with a variety of GGA and hybrid functionals (PW91, BP86, OLYP and B3LYP), to see which functional could correctly predict the experimental S = 5/2 state [28]. The relative energies are given in Table 3. OLYP and B3LYP successfully predicted a sextet ground state (Table 3). PW91 and BP86, however, incorrectly predicted a doublet state, with the sextet state about 0.30–0.44 eV higher in energy. This result is in agreement with the finding of others [29] that early GGA functionals, like BP86, tend to overstabilize the low-spin state, the hybrid functionals, like B3LYP, tend to overstabilize the high-spin state (due to the inclusion of a portion of Hartree-Fock exchange), while OPBE (and the related OLYP) seems to be giving good results not only for iron complexes but also for other transition metals.

Rotation of the thienyl group in [Fe(tta)$_3$] did not have a significant influence on the energy of either the *fac* or *mer* ground states of [Fe(tta)$_3$], as long as the five-membered ring stayed co-planar with the plane through the backbone of the β-diketonato ligand, to which it is attached. This co-planar orientation enhances electronic conjugation between the five-membered ring and the backbone of the β-diketonato ligand. This result is in agreement with the *ca*. 80% *anti* : 20% *syn* disorder found in the structure of [Fe(tta)$_3$] (**1**, isomer *fac*). However, the optimized geometry of [Fe(tffu)$_3$] (**2**), with the furyl group in a *syn* orientation, is 0.3 eV more stable than the optimized geometry of [Fe(tffu)$_3$] (**2**), with the furyl group in an *anti* orientation, predicting that the *syn* orientation is preferred, as has been found experimentally.

To further validate the DFT computational method, the calculated bond lengths and bond angles of [Fe(acac)$_3$], [Fe(tta)$_3$] (**1**) (*fac* and *mer*) and [Fe(tffu)$_3$] (**2**) (*fac* and *mer*) (S = 5/2), obtained by a selection of functionals, were compared to experimental crystal data (Table 4). The bond lengths

and angles involving the metal centre were of primary importance. The average experimental Fe–O bonds in [Fe(acac)$_3$] of 1.99(1) Å, as obtained from ten experimental crystal structures, are slightly overestimated by 0.04–0.07 Å for the calculated bonds, which would have been expected, since GGA density functionals tend to overestimate bonds lengths [30]. Longer calculated bond lengths, compared to crystallographic measured bond lengths, have also been found for square planar metal β-diketonato complexes [31]. The calculated O–Fe–O angle of [Fe(acac)$_3$], is within 1.1° of the average experimental value. A good agreement between the experimental and calculated bond lengths were also found for [Fe(tta)$_3$] (**1**) *fac* isomer, [Fe(tta)$_3$] (**1**) *mer* isomer, and [Fe(tffu)$_3$] (**2**) *mer* isomer, where the calculated bond lengths were slightly overestimated by 0.01–0.06 Å for PW91, BP86 and B3LYP, and by 0.01–0.12 Å for OLYP. The angles around the Fe atom were calculated accurately, within 0.8° for PW91, BP86 and B3LYP, and within 2.4° for OLYP. Since comparisons of experimental bond lengths with calculated bond lengths, below threshold of 0.02 Å are considered as meaningless [32], the PW91, BP86 and B3LYP functionals used in this study, all give a good agreement with experimental geometric parameters, while OLYP performed the worst. However, PW91 and BP86 calculations did not give the sextet ground state. Therefore B3LYP is considered to be the best functional in calculating both the energy and geometry of tris(β-diketonato) iron(III) systems related to this study. The B3LYP optimized geometries of both the facial isomer (*fac*) and meridional isomer (*mer*) of [Fe(tta)$_3$] (**1**) and [Fe(tffu)$_3$] (**2**) are given in Figure 5.

Table 3: Relative energies (eV) of the different spin states (default occupations) of [Fe(acac)$_3$], [Fe(tta)$_3$] (**1**) and [Fe(tffu)$_3$] (**2**), with a selection of functionals.

Spin	**PW91**	**BP86**	**OLYP**	**B3LYP**
[Fe(acac)$_3$]				
1/2	**0.00**	**0.00**	0.58	1.35
3/2	0.66	0.62	0.78	1.45
5/2	0.37	0.30	**0.00**	**0.00**
[Fe(tta)$_3$] (**1**) *fac*				
1/2	**0.00**	**0.00**	0.55	0.37
3/2	0.57	0.54	0.68	0.63
5/2	0.43	0.34	**0.00**	**0.00**
[Fe(tta)$_3$] (**1**) *mer*				
1/2	**0.00**	**0.00**	0.52	0.46
3/2	0.58	0.56	0.65	0.67
5/2	0.43	0.36	**0.00**	**0.00**
[Fe(tffu)$_3$] (**2**) *fac*				
1/2	**0.00**	**0.00**	0.54	0.45
3/2	0.57	0.54	0.66	0.67
5/2	0.44	0.35	**0.00**	**0.00**
[Fe(tffu)$_3$] (**2**) *mer*				
1/2	**0.00**	**0.00**	0.51	0.48
3/2	0.56	0.53	0.63	0.67
5/2	0.43	0.35	**0.00**	**0.00**

Table 4: Selected experimental and calculated geometrical parameters of high-spin (S = 5/2) complexes $[Fe(acac)_3]$, $[Fe(tta)_3]$ (**1**) and $[Fe(tffu)_3]$ (**2**), with a selection of functionals. For the Fe–O bond lengths, the average of the 3 related bonds (near CF_3 or near thienyl/furyl) are given.

Properties	**PW91**	**BP86**	**OLYP**	**B3LYP**	**Crystal**	**reference crystal data**
$[Fe(acac)_3]$						[33]
Fe–O (Å)	2.034	2.036	2.059	2.031	1.99(1) [a]	
O–Fe–O (°)	87.2	87.0	86.2	87.9	87.3(9) [a]	
$[Fe(tta)_3]$ (**1**) *fac*						this study
Fe–O near CF_3 (Å)	2.022(1)	2.025(1)	2.052(0)	2.001(0)	1.974(0)	
Fe–O near thienyl (Å)	2.043(0)	2.041(0)	2.068(0)	2.061(0)	1.995(0)	
O–Fe–O (°)	86.7(0)	86.8(0)	85.1(0)	86.7(0)	87.5(0)	
$[Fe(tta)_3]$ (**1**) *mer*						[9]
Fe–O near CF_3 (Å)	2.036(8)	2.032(4)	2.09(3)	2.02(2)	1.98(2)	
Fe–O near thienyl (Å)	2.03(1)	2.035(5)	2.03(2)	2.03(2)	2.01(2)	
O–Fe–O (°)	86.6(5)	86.7(3)	85.1(8)	87.0(5)	87(1)	
$[Fe(tffu)_3]$ (**2**) *fac*						-
Fe–O near CF_3 (Å)	2.022(0)	2.027(0)	2.057(1)	2.018(0)	-	
Fe–O near furyl (Å)	2.039(0)	2.037(0)	2.061(0)	2.039(0)	-	
O–Fe–O (°)	87.0(0)	87.1(0)	85.4(0)	87.4(0)	-	
$[Fe(tffu)_3]$ (**2**) *mer*						this study
Fe–O near CF_3 (Å)	2.04(1)	2.035(9)	2.10(3)	2.03(1)	1.986(7)	
Fe–O near furyl (Å)	2.02(1)	2.03(1)	2.02(2)	2.02(1)	2.008(4)	
O–Fe–O (°)	86.8(4)	86.9(3)	85.3(8)	87.5(3)	87.6(4)	

a Average value obtained from 10 crystals from CSD, see reference [33].

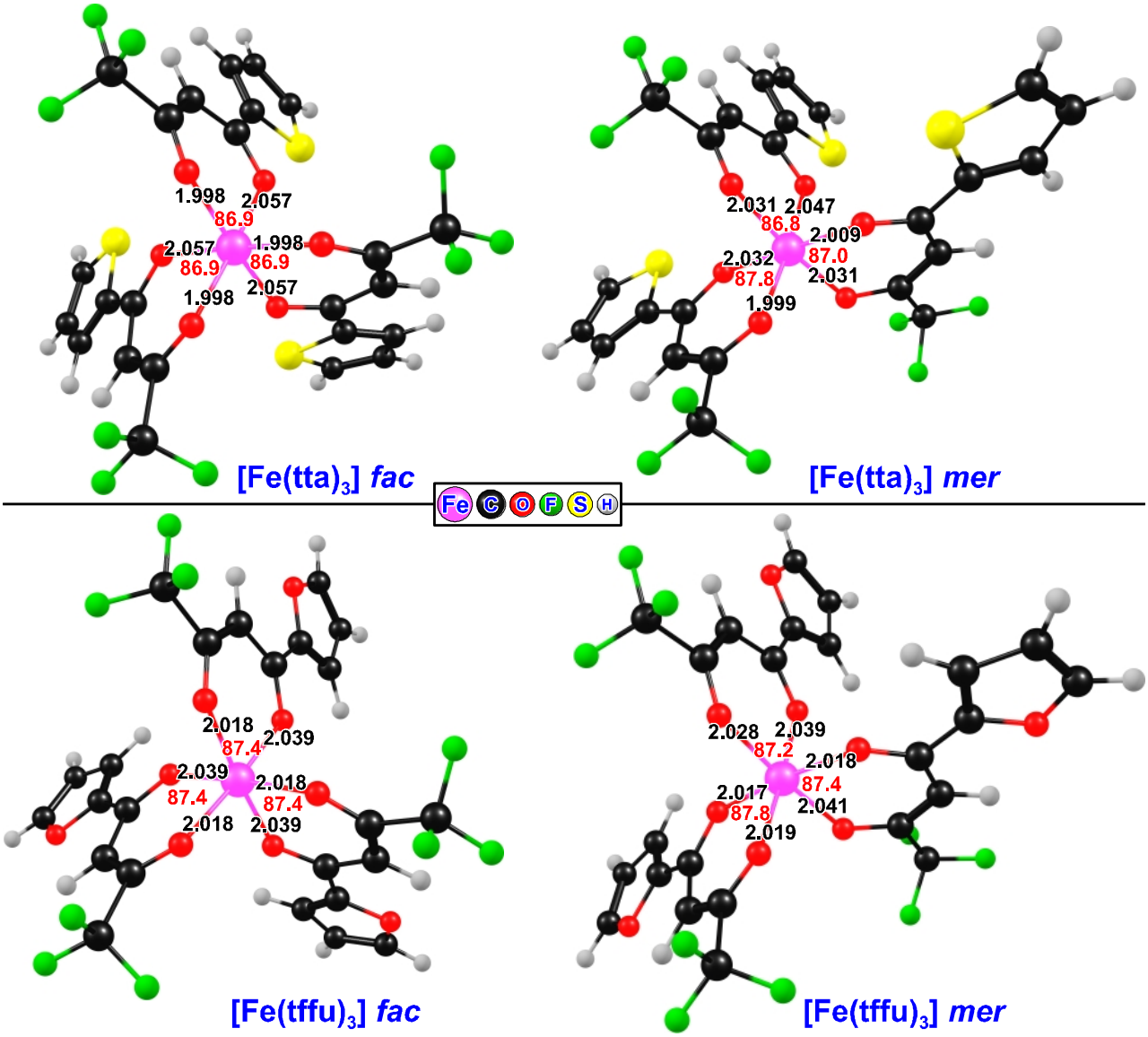

Figure 5: B3LYP optimized geometries of the *fac* and *mer* isomers of (**1**) and (**2**). The distances (Å, black), the angles (°, red) and the colour code of the atoms are as indicated.

Distortion from the octahedral orbital energies (O_h) towards D_3 ligand symmetry, splits the degenerate t_{2g}-orbitals into *a* and *e* components. A positive D_3 distortion has the *e* component lower in energy than *a*. A negative distortion has the *a* component lower in energy than *e*. ADF results showed, that complex [Fe(acac)$_3$] exhibits a negative distortion, with the lowest *d*-orbital having *a* symmetry; see the molecular energy level diagram of [Fe(acac)$_3$] in Figure 6. Note that the high-spin [Fe(acac)$_3$] complex has five unpaired electrons and therefore both the α ("up" spin) and β ("down" spin) are included in this figure. This distortion is observed in the arrangement of the molecular energy levels, not in the physical geometry of [Fe(acac)$_3$]. The geometry of [Fe(acac)$_3$] does not exhibit Jahn-Teller distortion, since the *e* orbitals are doubly degenerate.

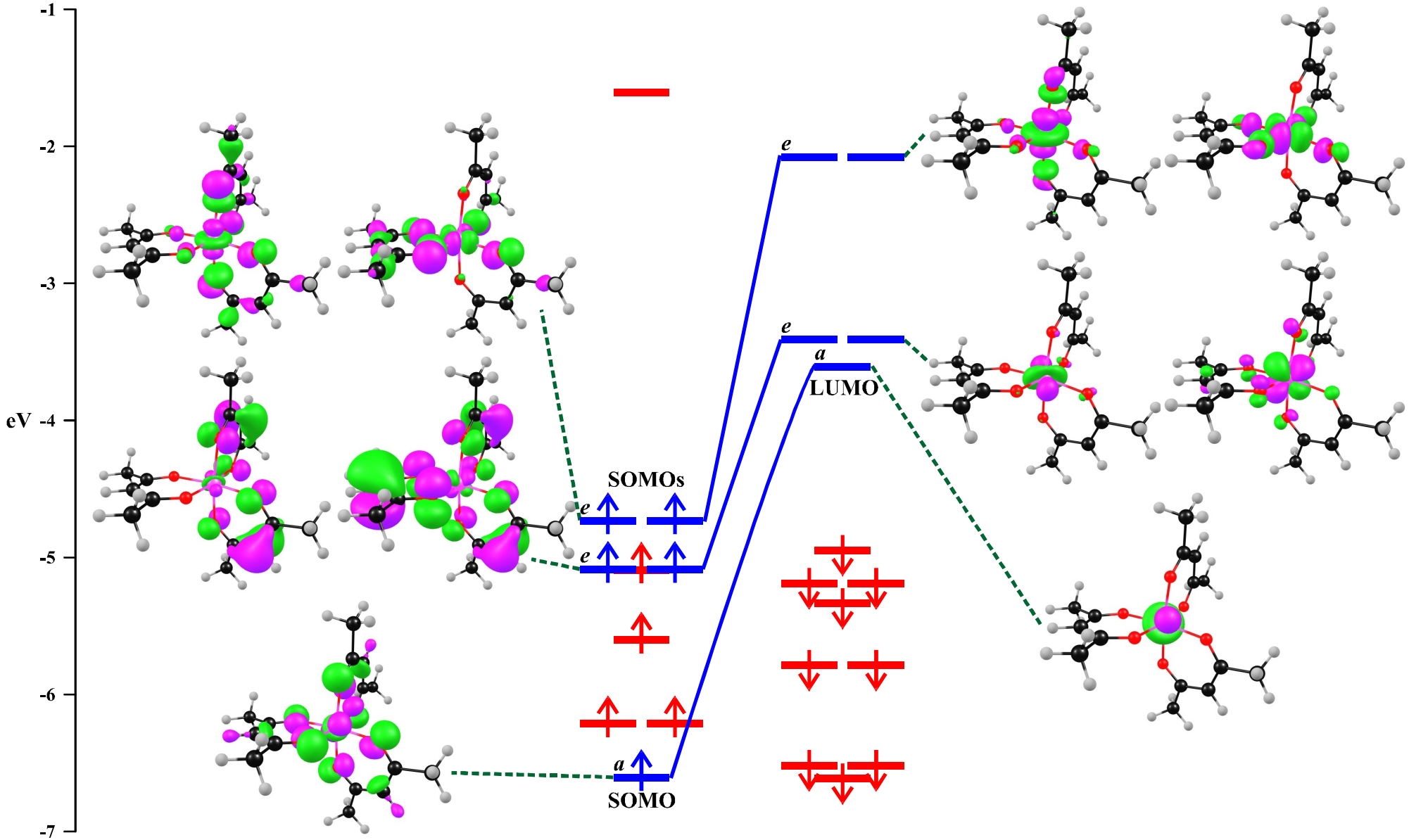

Figure 6: Molecular orbital Kohn-Sham energy levels (eV) for $[Fe(acac)_3]$, with S = 5/2. The *d*-based MOs are shown in blue, whereas the MOs concentrated largely on the supporting β-diketone ligands, are indicated in red. The MOs of α *d*-orbitals are illustrated on the left of the figure, and the β *d*-orbitals are illustrated on the right.

The ratios of the *fac : mer* isomers, calculated by the Boltzmann equation for the different functionals, are given in Table 5. It is interesting to note that all functionals predict the *mer* isomer as the main isomer for both [Fe(tta)$_3$] and [Fe(tffu)$_3$]. The *mer* isomer of [Fe(tta)$_3$] has been published previously, while the minor *fac* isomer of [Fe(tta)$_3$] is presented in this study. Since the complexes of this study are paramagnetic, it is not possible to measure the *fac : mer* ratio experimentally by NMR. Due to the fact that B3LYP is known to overstabilize the high-spin state [29], while OLYP also gives reliable energy values for the complexes of this study, the OLYP calculated population might be more realistic in view of the fact that it was possible to isolate the minor *fac* isomer of [Fe(tta)$_3$]. [Fe(tta)$_3$] is the first tris(β-diketonato) iron(III) complex for which both the fac and mer isomer is characterized by solid X-ray crystallography, according to the CSD [34].

Table 5: Calculated Boltzmann population (%) of the *fac* and *mer* isomers of [Fe(tta)$_3$] (**1**) and [Fe(tffu)$_3$] (**2**), as obtained from calculations with a selection of functionals (T = 298.15 K).

	PW91	**BP86**	**OLYP**	**B3LYP**
[Fe(tta)$_3$] (**1**) *fac*	33.1	34.4	32.4	1.9
[Fe(tta)$_3$] (**1**) *mer*	66.9	65.6	67.6	98.1
[Fe(tffu)$_3$] (**2**) *fac*	10.2	18.4	23.7	6.2
[Fe(tffu)$_3$] (**2**) *mer*	89.8	81.6	76.3	93.8

4 Conclusions

DFT calculations showed that both the *fac* and *mer* isomers of [Fe(tta)$_3$] and [Fe(tffu)$_3$] can exist, although the *mer* isomer is energetically favoured to be the major isomer. The crystal structures of the minor *fac* isomer [Fe(tta)$_3$] and the major *mer* of [Fe(tffu)$_3$], are presented in this study. DFT calculations further showed no preferred *syn* or *anti* orientation of the thienyl group in [Fe(tta)$_3$] (**1**), while the *syn* orientation of the furyl group in [Fe(tffu)$_3$] (**2**) is preferred. Experimentally the thienyl group in [Fe(tta)$_3$] (**1**) showed a 80 : 20 *anti : syn* disorder, while the furyl group in [Fe(tffu)$_3$] (**2**) has a *syn* orientation. The hybrid functional B3LYP provided the best description of both the spin state and geometry of Fe(β-diketonato)$_3$ complexes, compared to the other functionals tested in this study.

Supporting Information

Crystallographic data has been deposited at the Cambridge Crystallographic Data Centre with numbers: **1** (950662), **2** (950663). Copies can be obtained, free of charge, on application to CCDC, 12 Union Road, Cambridge CB2 1EZ, UK [fax: +44 (0)1223 336033 or ww.ccdc.cam.ac.uk/products/csd/request/]. The optimized coordinates of the DFT calculations are given in the Supporting Information.

Acknowledgements

This work has received support from the Norwegian Supercomputing Program (NOTUR) through a grant of computer time (Grant No. NN4654K), the South African National Research Foundation and the Central Research Fund of the University of the Free State, Bloemfontein.

References

1 K.T. Williamson and T. Yoon, J. Am. Chem. Soc., 132 (2010) 4570–4571.

2 A. Misono, Y. Uchida, M. Hidai and Y. Ohsawa, Bull. Chem. Soc. Jpn., 39 (1966) 2425-2429.

3 M. Tamura and J. Kochi, J. Am. Chem. Soc., 93 (1971) 1487-1489.

4 C.M. Rao Volla and P. Vogel, Angew. Chem. Int. Ed., 47 (2008) 1-4.

5 A. Sudo, S. Hirayama and T. Endo, J. Polym. Sci., Part A: Polym. Chem., 48 (210) 479-484.

6 S.M. Neumann and J.K. Kochi, J. Org. Chem., 40 (1975) 599-606.

7 E.W. Berg and J.T. Truemper, J. Phys. Chem., 64 (1960) 487-490.

8 (a) K. Endo, M. Furukawa, H. Yamatera and H Sano, Bull. Chem. Soc. Jpn., 53 (1980) 407-410. (b) G.S. Hammond, D.C. Nonhebel and C.S. Wu, Inorg. Chem., 2 (1963) 73-76.

9 H. Soling, Acta Chem. Scand. A, 30 (1976) 163-170.

10 G. te Velde, F.M Bickelhaupt, E.J. Baerends, C. Fonseca Guerra, S.J.A. van Gisbergen, J.G. Snijders and T. Ziegler, J. Comput. Chem., 22 (2001) 931-967.

11 J.P. Perdew, J.A. Chevary, S.H. Vosko, K.A. Jackson, M.R. Pederson, D.J. Singh and C. Fiolhais, Phys. Rev. B, 46 (1992) 6671-6687. Erratum: J.P. Perdew, J.A. Chevary, S.H. Vosko, K.A. Jackson, M.R. Perderson, D.J. Singh and C. Fiolhais, Phys. Rev. B, 48 (1993) 4978.

12 A.D. Becke, Phys. Rev., A38 (1988) 3098-3100.

13 J.P. Perdew, Phys. Rev., B33 (1986) 8822-8824; Erratum: J.P. Perdew, Phys. Rev., B34 (1986) 7406.

14 N.C. Handy and A.J. Cohen, Mol. Phys., 99 (2001) 403-412.

15 (a) C. Lee, W. Yang and R.G. Parr, Phys. Rev. B, 37 (1988) 785-789. (b) B.G. Johnson, P.M.W. Gill and J.A. Pople, J. Chem. Phys., 98 (1993) 5612-5626. (c) T.V. Russo, R.L. Martin and P.J. Hay, J. Chem. Phys., 101 (1994) 7729-7737.

16 A.D. Becke, J.Chem.Phys., 98 (1993) 5648-5652.

17 P.J. Stephens, F.J. Devlin, C.F. Chabalowski and M.J. Frisch, J.Phys.Chem. 98 (1994) 11623-11627.

18 E. van Lenthe, A.E. Ehlers and E.J. Baerends, J. Chem. Phys., 110 (1999) 8943-8953.

19 E. van Lenthe, E.J. Baerends and J.G. Snijders, J. Chem. Phys., 99 (1993) 4597-4610.

20 E. van Lenthe, E.J. Baerends and J.G. Snijders, J. Chem. Phys., 101 (1994) 9783-9792.

21 E. van Lenthe, J.G. Snijders and E.J. Baerends, J. Chem. Phys., 105 (1996) 6505-6516.

22 E. van Lenthe, R. van Leeuwen, E.J. Baerends and J.G. Snijders, Int. J. Quantum Chem., 57 (1996) 281-293.

23 APEX2 (including SAINT and SADABS); Bruker AXS Inc., Madison, WI, 2012

24 G. M. Sheldrick, Acta Cryst., A64 (2008) 112-122.

25 L.J. Farrugia, *J. Appl. Crystallogr.*, 45 (2012) 849-854.

26 F.A. Cotton, G. Wilkinson, C.A. Murillo, M. Bochmann, Advanced inorganic chemistry, Sixth edition, John Wiley & Sons, New York, 1999, p790.

27 I. Diaz-Acosta, J. Baker, W. Cordes and P. Pulay, J. Phys. Chem. A, 105 (2001) 238-244.

28 M. Gerloch, J. Lewis and R. C. Slade, J. Chem. Soc. A (1969) 1422-1427.

29 (a) M. Swart, J. Chem. Theory Comput. 4 (2008) 2057–2066 (b) M. Swart, A.R. Groenhof, A.W. Ehlers, K. Lammertsma, J. Phys. Chem. A 108 (2004) 5479-5483 (c) J. Conradie, A. Ghosh, J. Phys. Chem. B 111 (**2007)** 12621-12624 (d) J. Conradie, A. Ghosh, J. Chem. Theory Comput. 3 (**2007)** 689-702.

30 (a) A.C. Scheiner, J. Baker and J.W. Andzelm, J. Comput. Chem., 18 (1997) 775-795. (b) J.R. Hill, C.M. Freeman and B. Delley, J. Phys. Chem. A, 103 (1999) 3772-3777. (c) F. Furche and J.P. Perdew, J. Chem Phys., 124 (2006) 044103-044129.

31 (a) M.M. Conradie and J. Conradie, Inorg. Chim. Acta 362 (2009) 519-530. (b) M.M. Conradie and J. Conradie, S. Afr. J. Chem.61 (2008) 102-111.

32 W.J. Hehre, A Guide to Molecular Mechanisms and Quantum Chemical Calculations, Wavefunction Inc., (2003) p153.

33 Average value for 10 crystals from CSD, reference codes: FEACAC02, FEACAC02, FEACAC03, FEACAC05, FEACAC07, FEACAC08, FEACAC09, JICMEN, JICMEN01, VUBSOA. Cambridge Structural Database (CSD), Version 534, November 2012 update.

34 Cambridge Structural Database (CSD), Version 5.34, May 2013 update.